

**Supporting Information for**

**Observation of Three Different Linker Conformers in a Scandium  
Ferrocenedicarboxylate Coordination Polymer**

Jannik Benecke<sup>a</sup>, Erik Svensson Grape<sup>b</sup>, Tobias A. Engesser<sup>a</sup>, A. Ken Inge<sup>b</sup> and Helge  
Reinsch<sup>a\*</sup>.

<sup>a</sup>Institute of Inorganic Chemistry, Christian-Albrechts-Universität, Max-Eyth Straße 2,  
D-24118 Kiel, Germany

<sup>b</sup>Department of Materials and Environmental Chemistry, Stockholm University, SE-106 91  
Stockholm, Sweden

## Index

1. Characterisation Methods.....	3
1.1 Powder X-Ray Diffraction .....	3
1.2 IR Spectroscopy .....	3
1.3 UV/VIS Spectroscopy .....	3
1.4 EDX and ESEM .....	3
1.5 CHN Analysis.....	3
1.6 Thermogravimetry.....	3
1.7 N <sub>2</sub> and H <sub>2</sub> O Sorption Measurements.....	3
1.8 EPR Spectroscopy .....	3
1.9 Mössbauer Spectroscopy .....	3
1.10 Electron Diffraction .....	4
1.11 Cyclic Voltammetry .....	4
2 Synthesis and Chemicals.....	5
3D Electron Diffraction Data .....	6
4 Rietveld Refinement.....	7
5 Structures .....	9
6 SEM.....	11
7 EDX Analysis.....	11
8 TG Analysis.....	12
9 CHN Analysis.....	13
10 Variable Temperature Powder X-ray Diffraction.....	14
11 IR Spectroscopy .....	15
12 UV/VIS Spectroscopy .....	16
13 EPR Spectroscopy .....	17
14 Mössbauer Spectroscopy .....	18
15 Sorption .....	18
16 Cyclic Voltammetry .....	20

## 1. Characterisation Methods

### 1.1 Powder X-Ray Diffraction

Different powder diffractometers were used in this work. For high resolution and PXRD measurements after sorption and thermogravimetric experiments, a STOE Stadi-MP powder diffractometer (Cu K $\alpha$ 1 radiation) was used. Furthermore, the variable temperature (VT) PXRD measurements were performed in transmission geometry with a STOE Stadi-P combi powder diffractometer (Cu K $\alpha$ 1 radiation) equipped with a capillary furnace. Therefore the samples were placed in 0.5 mm quartz capillaries. The PXRD experiments of the MOF deposited on gold electrodes were performed with a Panalytical X'Pert Pro MPD equipped with Göbel mirror and a PIXCel 1D detector using Cu K $\alpha$  radiation in reflection geometry.

### 1.2 IR Spectroscopy

The IR spectra of the samples were recorded with a Bruker ALPHA-FT-IR A220/D-01 spectrometer using an ATR-unit.

### 1.3 UV/VIS Spectroscopy

The UV/VIS spectra were recorded with an Agilent UV/VIS-NIR spectrometer in reflection geometry. Prior to the measurement the powders were mixed with BaSO<sub>4</sub>.

### 1.4 EDX and ESEM

The EDX measurements were performed with an Apollo XL detector. Micrographs were recorded using a Philips ESEM XL 30.

### 1.5 CHN Analysis

CHN contents were determined with a vario MICRO cube element analyzer of the company Elementar.

### 1.6 Thermogravimetry

The thermogravimetric measurements were performed using a NETZSCH STA 409 CD analyser. The flow of air was adjusted to 75 mL/min. The heating rate for the TG measurement amounts to 4°C/min.

### 1.7 N<sub>2</sub> and H<sub>2</sub>O Sorption Measurements

The sorption experiments were performed with a BEL Japan Inc. BELSORP-max using Nitrogen (77 K) and water vapour (298 K).

### 1.8 EPR Spectroscopy

All EPR spectra were measured with a Bruker EMXplus spectrometer with a PremiumX microwave bridge and a Bruker HQ X-Band cavity. The experiments were performed at X-Band microwave radiation of 9.86 GHz. The microcrystalline powder was measured in solid state at room temperature.

### 1.9 Mössbauer Spectroscopy

The Mössbauer spectrum was measured on a custom made Mössbauer spectrometer. The spectrum was recorded in linear transmission geometry. As the power unit, the "Mössbauer Drive System MR206A" and the "Mössbauer Velocity Transducer MVT-1000" from the company "Wissenschaftliche Elektronik GmbH" in Starnberg were used. As the source of

radiation,  $^{57}\text{Co}$  in a Rhodium matrix with a starting activity of 25mCi was used. All shifts are denoted relative to  $\alpha$ -iron. The resulting spectrum was fitted with the software FitSuite 1.0.4.

### 1.10 Electron Diffraction

The data collection was conducted on a JEOL JEM-2100  $\text{LaB}_6$  transmission electron microscope, equipped with a Timepix hybrid electron detector. Data were collected through the help of Instamatic<sup>1</sup> while continuously tilting the specimen. The acquired frames were processed using XDS.<sup>2</sup> The structures were solved using SHELXT<sup>3</sup>, where all the non-hydrogen atoms could be located in the initial structure solutions. The crystallographic information as well as data statistics can be seen in Tables S1 and S2. Reciprocal lattice projections were constructed using the software REDp.<sup>4</sup>

### 1.11 Cyclic Voltammetry

The cyclic voltammograms were measured on an EG&G Princeton Applied Research/Model 273A using an Ag rod as a pseudo reference electrode and Pt as counter electrode. The MOF coated gold electrode consists of a glass substrate with a 50 $^\circ\text{\AA}$  titanium adlayer and a 200nm evaporated gold film on the surface. A solution of 0.01 mol/l  $\text{NaPF}_6$  in acetonitrile was used as electrolyte. As reference a minute amount of ferrocene was dissolved in the electrolyte and a CV was recorded with a blank gold electrode.

## 2 Synthesis and Chemicals

Scandium nitrate pentahydrate ( $\text{Sc}(\text{NO})_3 \cdot 5 \text{H}_2\text{O}$ , abcr, 99.9%) and 1,1'-ferrocenedicarboxylic acid ( $\text{H}_2\text{FcDC}$ , Alfa Aesar, 99%) were used as obtained and without further purification.

For the synthesis of CAU-50, scandium nitrate pentahydrate ( $\text{Sc}(\text{NO})_3 \cdot 5 \text{H}_2\text{O}$ ) (65.8 mg, 0.2050 mmol) and 1,1'-ferrocenedicarboxylic acid ( $\text{H}_2\text{FcDC}$ ) (56.5 mg, 0.2050 mmol) were used in a molar ratio of 1:1. Thereafter the reactants were placed in a Duran<sup>®</sup>-glass reactor (volume 8 mL). The solvent mixture of water (2 mL) and DMF (2 mL) and a stirring bar were added to the reactor. Afterwards the reactor was sealed and placed in an aluminium block and heated up to 95°C for 90 min under stirring. After the cooling process, the reaction product was filtered off and the orange powder was washed with 5 mL of DMF/water mixture (1:1). The powder was dried at room temperature in air overnight (yield: 66.2%). Afterwards the sample was stirred at room temperature in 5 mL MeOH overnight to remove residual solvent molecules.

## 3D Electron Diffraction Data

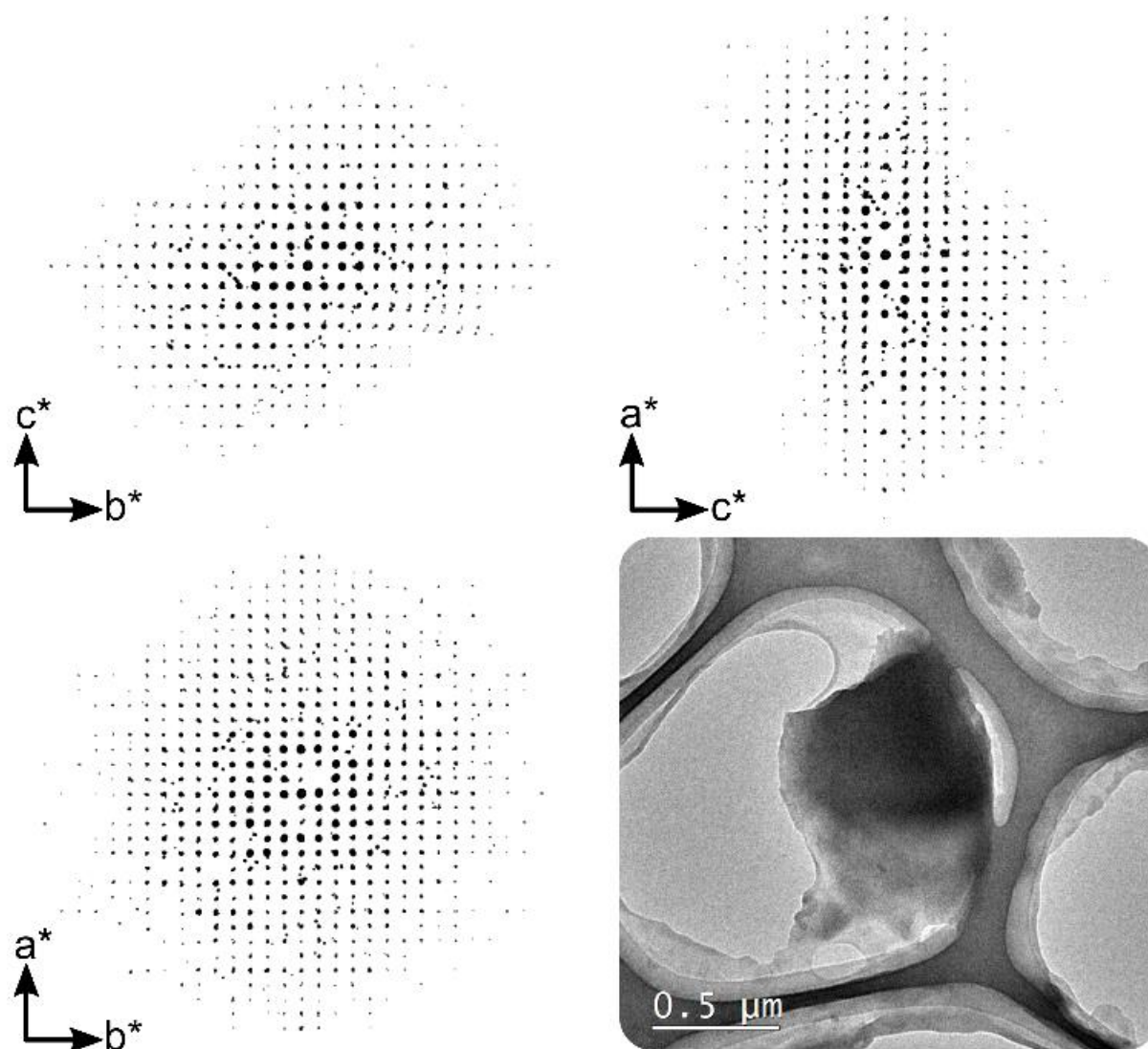


**Figure S1.** Reciprocal space projections of 3D ED data acquired from a crystal of CAU-50 (bottom right).

**Table S1.** Crystallographic table for 3D electron diffraction data of CAU-50.

Specimen	CAU-50
Crystal system	Orthorhombic
Space group	<i>Pnna</i> (No. 52)
Unit cell dimensions	$a = 18.05 \text{ \AA}$ $b = 15.90 \text{ \AA}$ $c = 13.54 \text{ \AA}$
Volume ( $\text{\AA}^3$ )	$3887 \text{ \AA}^3$
Z	4
Rotation range	$117.56^\circ$ ( $-56.63$ to $60.93^\circ$ )
Index ranges	$-22 \leq h \leq 22$ $-19 \leq k \leq 19$ $-16 \leq l \leq 16$
Reflections collected	15092
Independent reflections	3885 [R(int) = 0.2417]
Completeness (to 0.8 $\text{\AA}$ resolution)	98.0 %
$R_1$ (ED model) [ $I > 2\sigma(I)$ ]	0.2336

#### 4 Rietveld Refinement

The structure solution from electron diffraction data was used as starting point for further refinement based on PXRD data. Therefore the indexed cell parameters ( $a = 17.425(2) \text{ \AA}$ ,  $b = 15.292(2) \text{ \AA}$ ,  $c = 13.225(2) \text{ \AA}$ ) were imposed and the thus resulting model was optimised by force-field calculations using the Universal force field as implemented in the Material Studio software.<sup>5</sup> The resulting model was refined by Rietveld methods using TOPAS academics.<sup>6</sup> The organic units were treated as rigid bodies while all other atoms were freely refined using element specific temperature factors and distance restraints. The final Rietveld plot and some relevant parameters are summarised in Figure S2 and Table S2 below. Materials Studio was also used to generate a model bearing protons using the implemented “add hydrogen” option. The resulting model did not show any cavities accessible for molecules with the size of nitrogen. CCDC-2014713 contains the supplementary crystallographic data for this paper. These data can be obtained free of charge from the Cambridge Crystallographic Data Centre via [http://www.ccdc.cam.ac.uk/data\\_request/cif](http://www.ccdc.cam.ac.uk/data_request/cif).

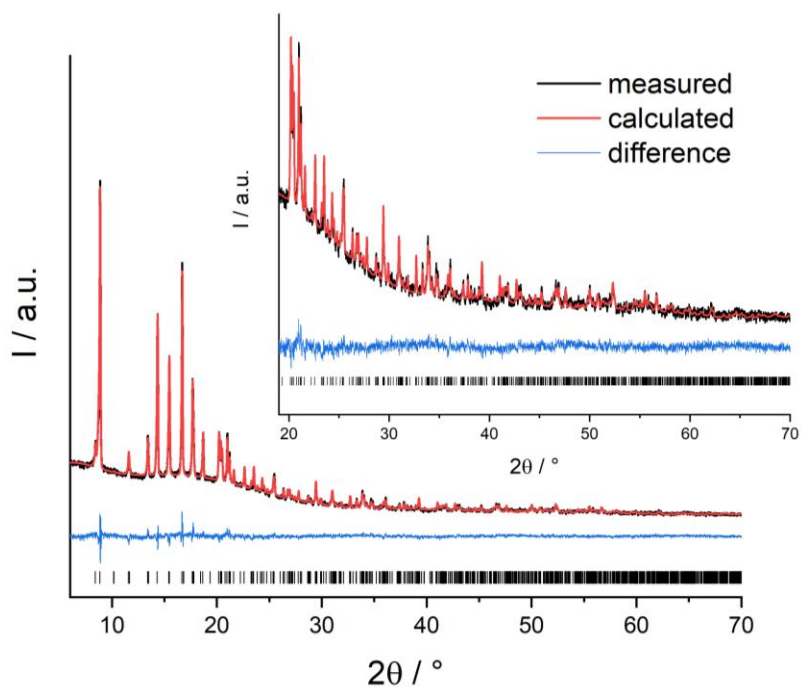


**Figure S2:** Rietveld-plot of CAU-50 with measured (black), calculated (red) and difference plots (blue). Vertical bars mark the allowed peak positions.

**Table S2.** Crystallographic table of CAU-50.

Compound	CAU-50
Formula sum	$[\text{Sc}_2(\text{O}_2\text{C}-\text{FeC}_{10}\text{H}_8-\text{CO}_2)_3]$
Space group	<i>Pnna</i>
Crystal system	orthorhombic
Cell parameters	$a = 17.4287(5) \text{ \AA}$ $b = 15.2905(5) \text{ \AA}$ $c = 13.2195(5) \text{ \AA}$
$R_{\text{WP}}$	2.5 %
GoF	1.8
$R_{\text{Bragg}}$	1.5 %

## 5 Structures

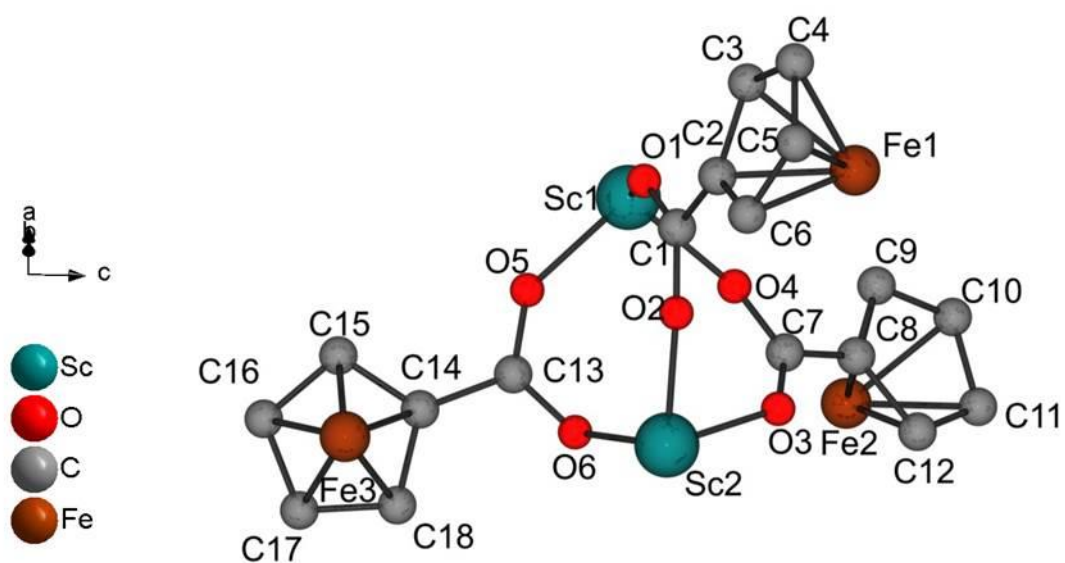


**Figure S3.** Asymmetric unit of the title compound.

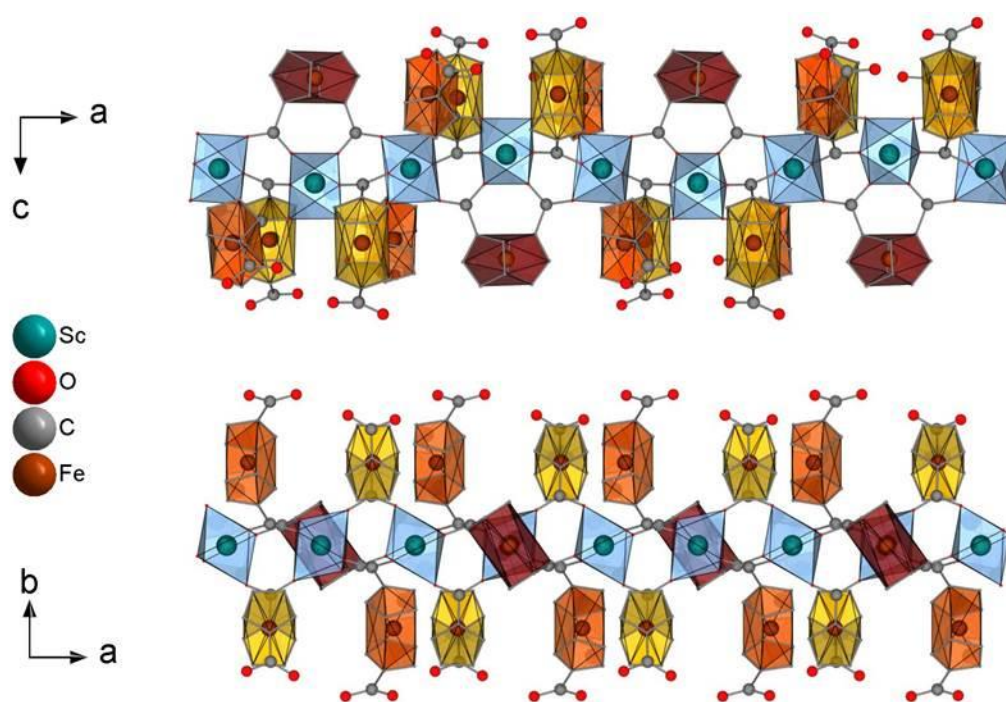


**Figure S4.** Representation of the coordinating linker molecules at the  $\text{ScO}_6$  octahedra of CAU-50 seen along the  $b$ -axis (top) and  $c$ -axis (bottom). The different conformers of  $\text{FcDC}^{2-}$  in the structure are shown as red (antiperiplanar), orange (anticlinal) and yellow polyhedra (synclinal).

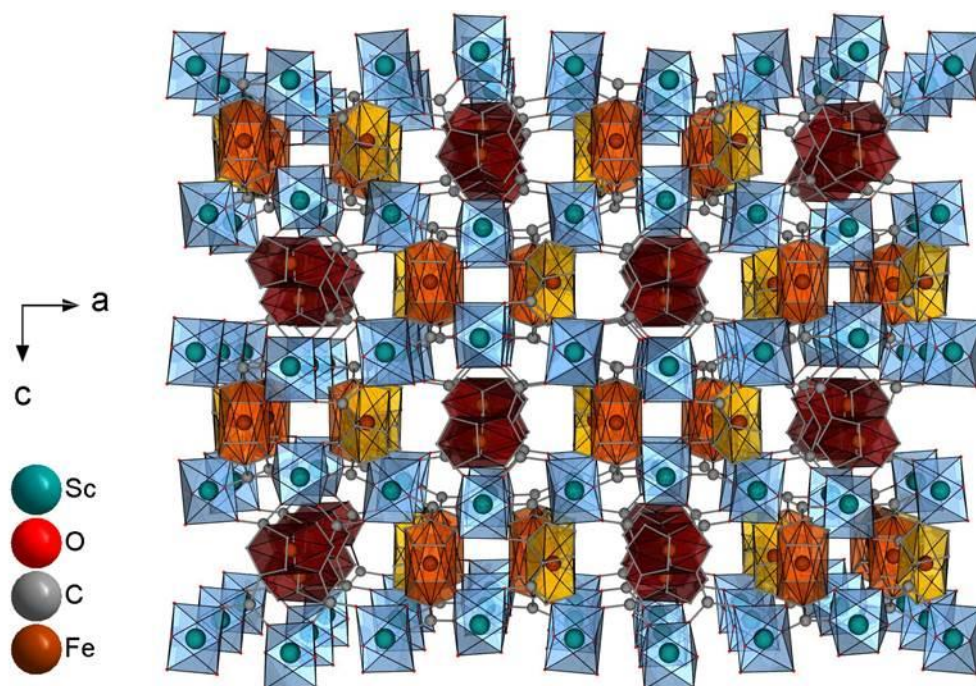


**Figure S5.** Representation of the structure of CAU-50 seen along the *b*-axis. The different conformers of FcDC<sup>2-</sup> in the structure are shown as red (antiperiplanar), orange (anticlinal) and yellow polyhedra (synclinal).

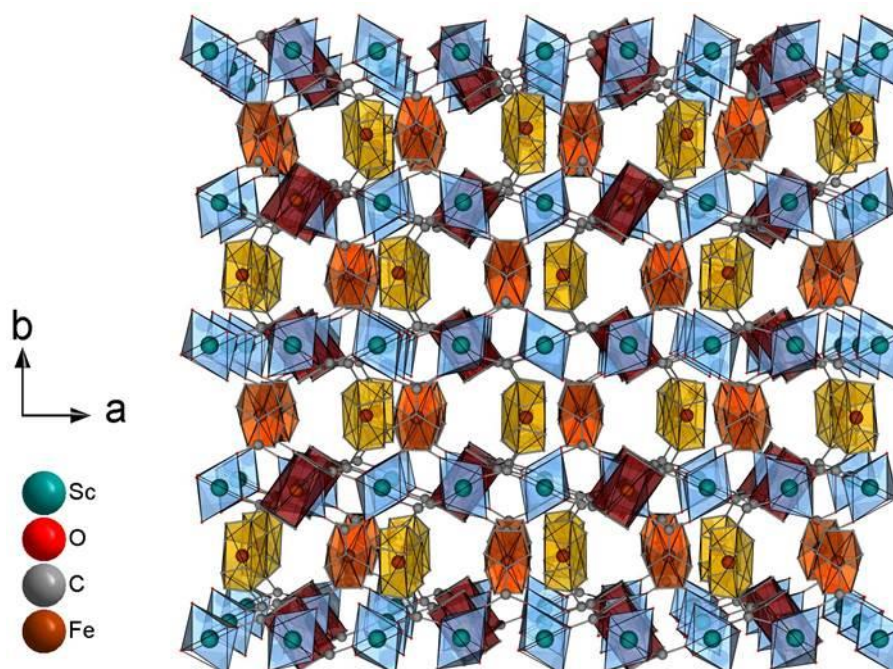


**Figure S6.** Representation of the structure of CAU-50 seen along the *c*-axis. The different conformers of FcDC<sup>2-</sup> in the structure are shown as red (antiperiplanar), orange (anticlinal) and yellow polyhedra (synclinal).

## 6 SEM



**Figure S7.** SEM Micrograph of CAU-50.

## 7 EDX Analysis

**Table S3.** Comparison of the measured and calculated Fe/Sc-Ratio of the title compound.

Sample	Fe-Ratio	Sc-Ratio
Calculated	1.5	1.0
1 <sup>st</sup> Measurement	1.5	1.0
2 <sup>nd</sup> Measurement	1.5	1.0
3 <sup>rd</sup> Measurement	1.5	1.0

## 8 TG Analysis

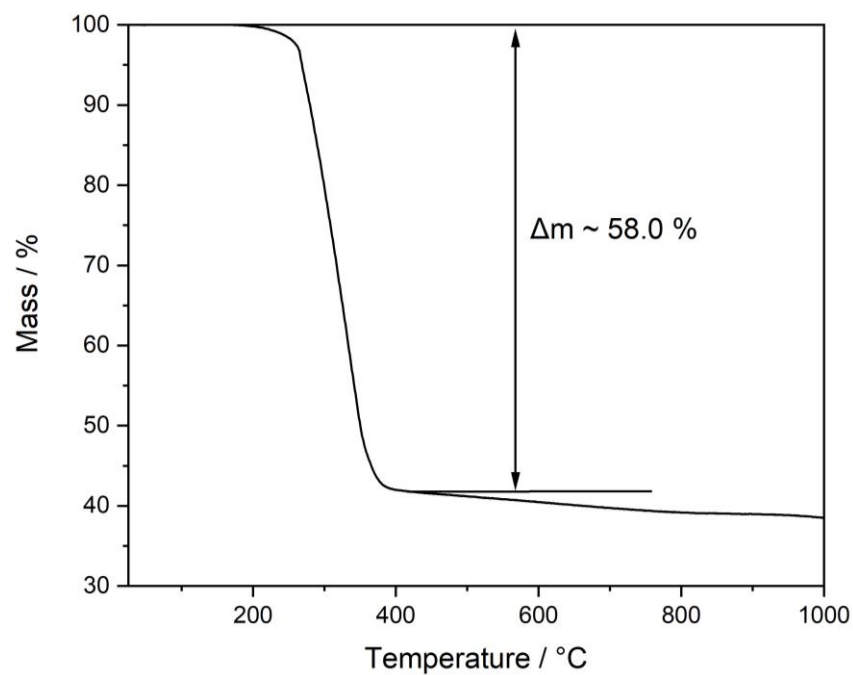


**Figure S8.** TG curve of CAU-50.

**Table S4.** Comparison of the measured and calculated mass loss observed in the TG curve of CAU-50. The calculated value is based on the formula  $[\text{Sc}_2(\text{FeC}_{12}\text{H}_8\text{O}_4)_3]$ .

TG	Measured / %	Calculated / %	
<b>CAU-50</b>			
<b>200 – 400 °C</b>	58.0	58.3	Linker decomposition
<b>Residue</b>	42.0	41.7	$\text{Sc}_2\text{O}_3 + \text{Fe}_2\text{O}_3$

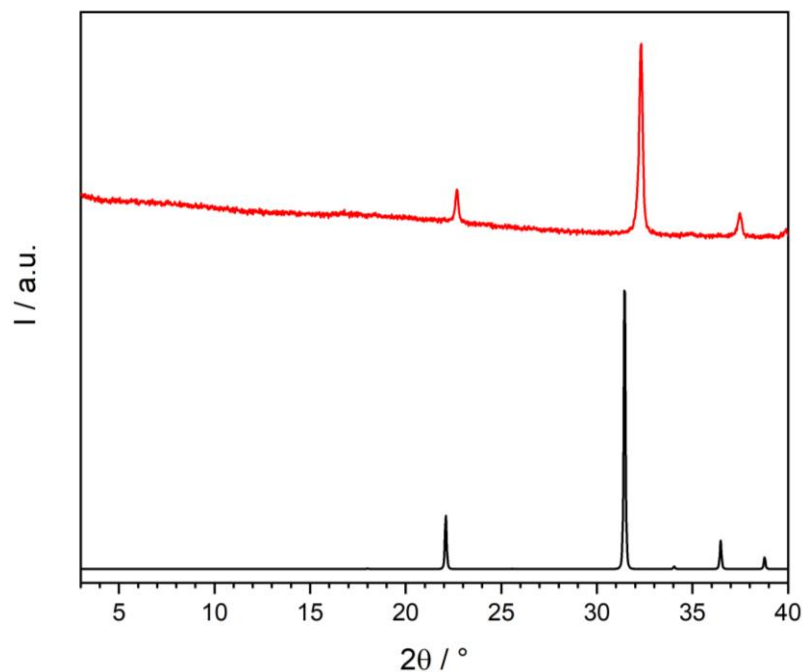


**Figure S9.** PXRD measurements of CAU-50 after TG measurement (red) and as comparison the calculated PXRD pattern of  $\text{Sc}_2\text{O}_3$  (black).<sup>7</sup> The small shift of the reflection to higher  $2\theta$  could be explained by a partial doping of  $\text{Sc}_2\text{O}_3$  with the smaller  $\text{Fe}^{3+}$  ions.

## 9 CHN Analysis

**Tab. S5** Comparison of the measured and calculated CHN values of CAU-50.

Compound	N / wt%	C / wt%	H / wt%
CAU-50	0.5	47.1	3.0
Calc. $[\text{Sc}_2(\text{FeC}_{12}\text{H}_8\text{O}_4)_3] \cdot 0.5 \text{H}_2\text{O} \cdot 0.7 \text{C}_3\text{H}_7\text{NO}$	0.7	47.3	3.0

## 10 Variable Temperature Powder X-ray Diffraction

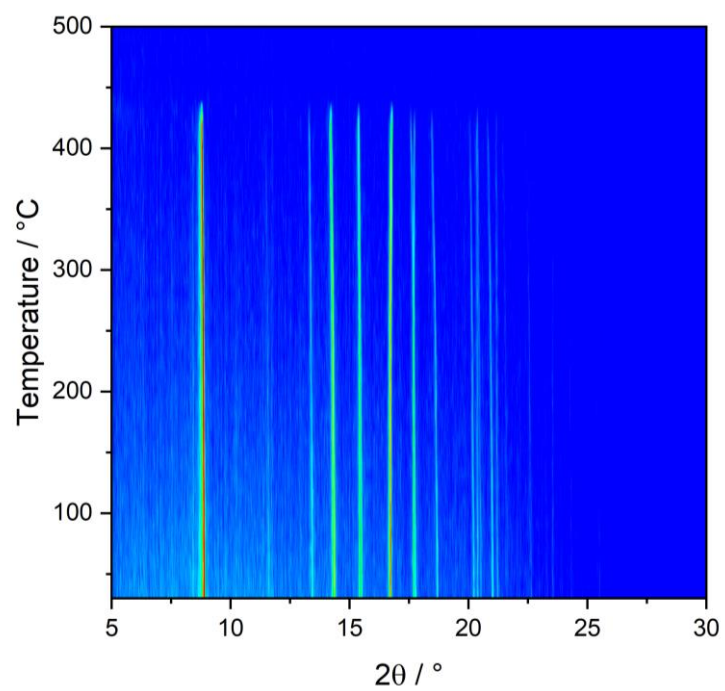


**Figure S10.** Results of the VT-PXRD measurement ( $\lambda = 1.5406 \text{ \AA}$ ) of CAU-50.

## 11 IR Spectroscopy

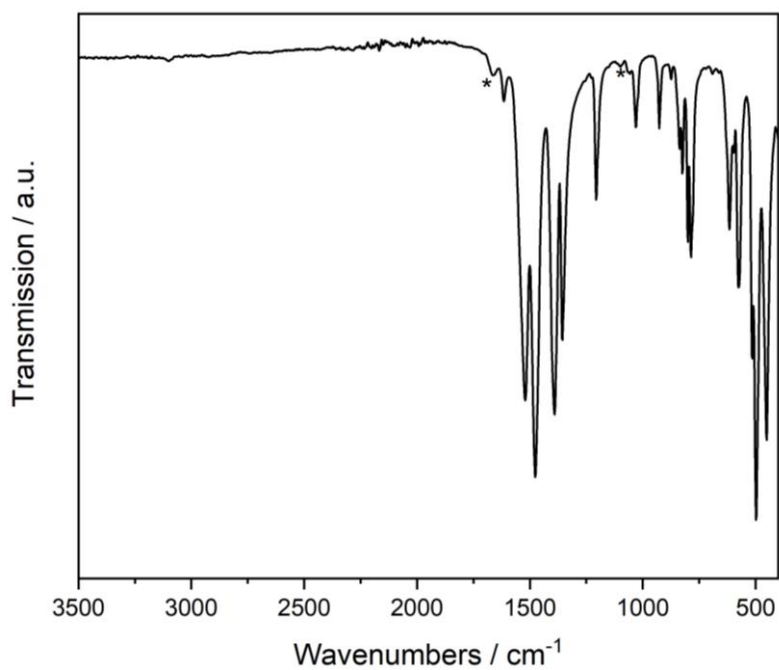


**Figure S11.** IR spectrum of CAU-50. The IR bands of traces of DMF molecules are labelled with asterisks.

**Table S6.** Assignment of the vibrational bands.<sup>8</sup>

Compound	Infrared Bands / $\text{cm}^{-1}$	Vibrations
CAU-50	3102	aromatic $\nu\text{C-H}$
	1673	$\nu\text{C=O}$ (DMF)
	1522	$\nu\text{C-O-O}$
	1472	$\nu\text{C=C}$
	1350	$\nu\text{C-O-O}$
	1091	$r\text{CH}_3\text{-N}$ (DMF)
	800	$\delta\text{C-H}$
	771	$\delta\text{C-H}$

## 12 UV/VIS Spectroscopy

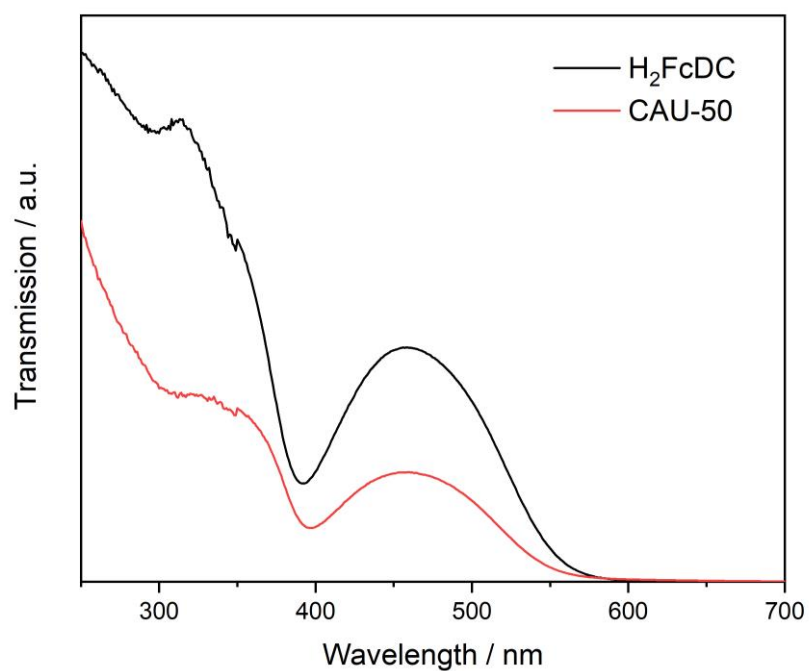


**Figure S12.** UV/VIS spectrum of CAU-50. In the UV/vis spectra of CAU-50, the absorption bands of the electronic transitions of the ferrocene complex could be clearly detected at 335 nm and 458 nm. For H<sub>2</sub>FcDC these transitions are located at 315 nm and 459 nm. According to the literature, the absorption bands of the corresponding electronic dd-transitions for pure ferrocene ( $^1A_{1g}$  to  $a^1E_{1g}$  and  $^1A_{1g}$  to  $b^1E_{2g}$ ) are observed at 325 nm and 440 nm.<sup>9</sup>

## 13 EPR Spectroscopy

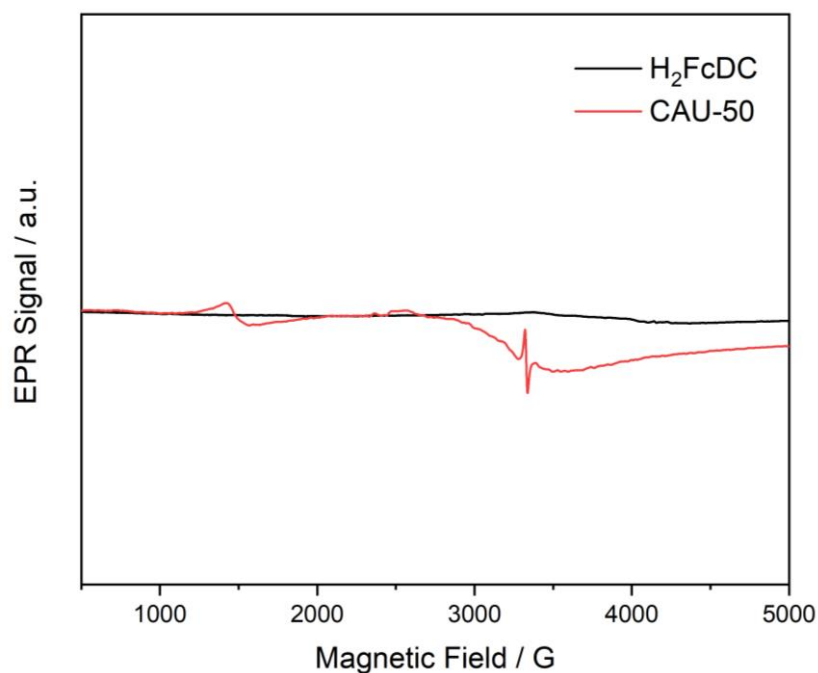


**Figure S13.** EPR spectra of CAU-50 (red) in comparison to the EPR silent H<sub>2</sub>FcDC (black). The spectrum of CAU-50 shows two different signals, at 1480 G (g-factor = 4.20) and a small second signal at 3335 G (g-factor = 2.00). The broad signal at smaller Gauss values can be assigned to traces of the oxidized linker molecule (ferroceniumdicarboxylate)<sup>10</sup> while the signal at higher Gauss values can be assigned to the presence of a negligibly small contamination with an organic radical.

## 14 Mössbauer Spectroscopy

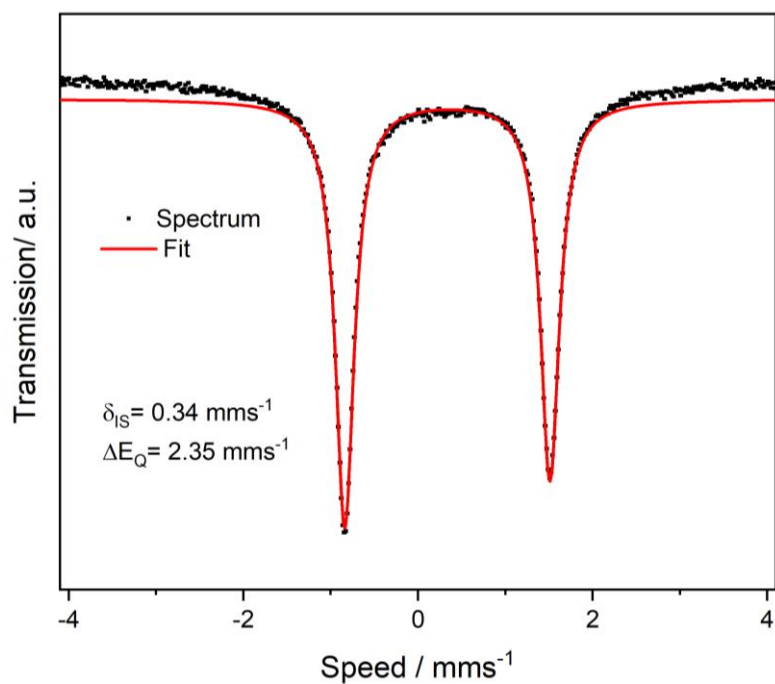


**Figure S14.** Mössbauer spectrum of CAU-50. The Mössbauer spectrum of the title compound shows a characteristic doublet with an isomeric shift of  $0.34 \text{ mms}^{-1}$  and a quadrupole splitting of  $2.35 \text{ mms}^{-1}$ , which is characteristic for ferrocene and the oxidation state +2 of the iron cation.<sup>11</sup>

## 15 Sorption

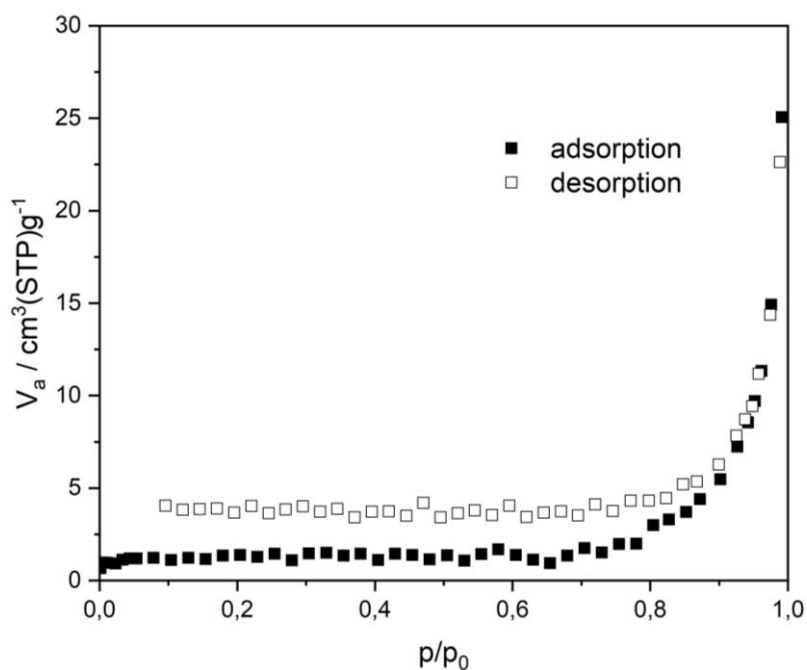


**Figure S15.**  $\text{N}_2$  sorption isotherm of CAU-50 at 77 K. For the sorption experiment the sample was activated at  $160 \text{ }^\circ\text{C}$  for 16h.

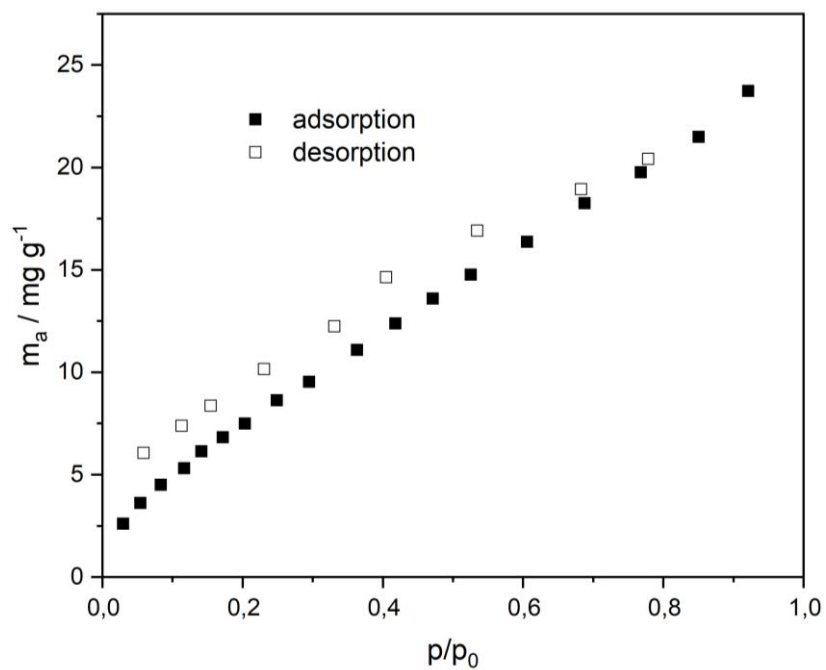


**Figure S16.** H<sub>2</sub>O sorption isotherm of CAU-50 at 298 K. For the sorption experiment the sample was activated at 120 °C for 16h.

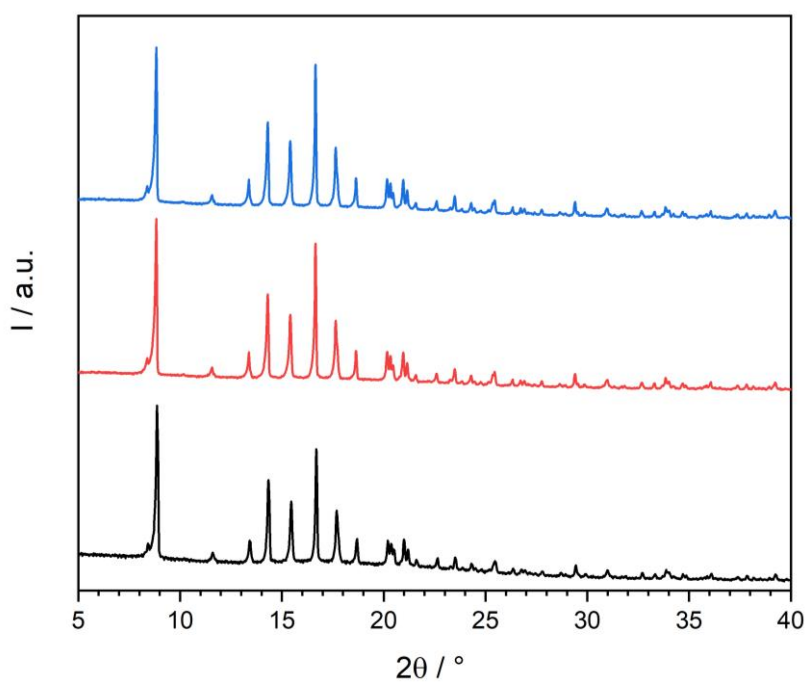


**Figure S17.** PXRD measurements of CAU-50 after N<sub>2</sub>-Sorption (red) and after H<sub>2</sub>O-Sorption (blue) in comparison to pristine CAU-50 (black).

## 16 Cyclic Voltammetry

CAU-50 was deposited in a matrix of the copolymer Nafion on the gold electrode. The gold electrodes were previously cleaned with 2-propanol by an ultrasonic bath treatment. The title compounds (8 mg) were dispersed in a solution consisting of ethanol, water and Nafion (1 mL, 6 mL and 30  $\mu$ l, respectively) in an ultrasonic bath for 30 min. Afterwards a liquid film of the dispersion was deposited on the electrode and dried in air over night. This procedure was repeated twice.

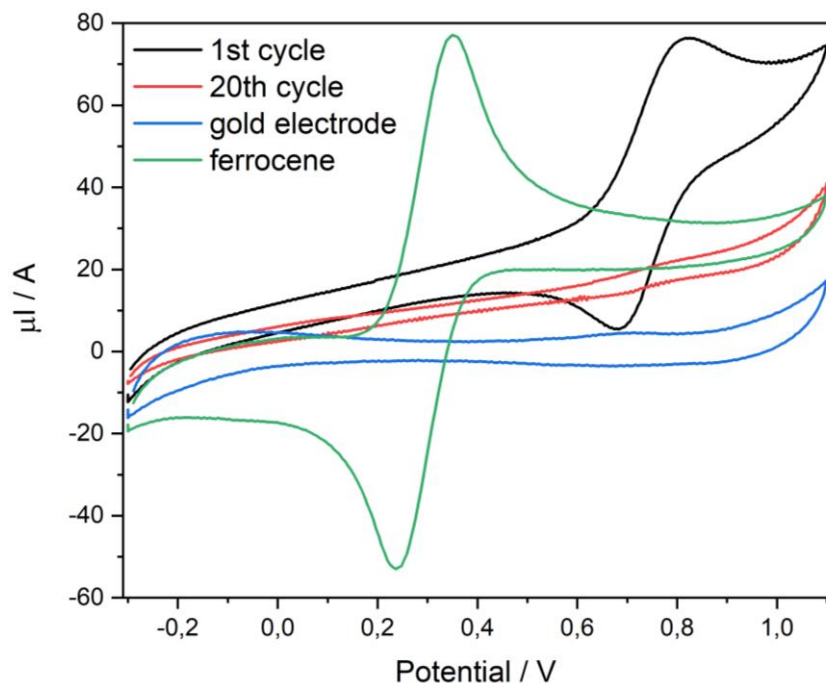


**Figure S18.** CV curve of CAU-50 on gold electrode: 1st cycle (black) and 20th cycle (red) using an Ag rod as a pseudo reference electrode. For comparison, the curves of the pure gold electrode (blue) and ferrocene in solution (green) are also shown. Solvent: acetonitrile, electrolyte: 0.01 mol/l NaPF<sub>6</sub>, working electrode: gold electrode, reference electrode: Ag rod and counter electrode: Pt rod

The reversible redox event, detected at 0.82 V (oxidation wave) and 0.68 V (reduction wave) can be assigned to the redox process of  $[\text{Fe}(\text{Cp})_2]/([\text{Fe}(\text{Cp})_2]^+)$ . The decreasing signal intensity of the oxidation and reduction waves can be explained by the progressive blocking process of the redox active center during the cycles. The washing process of the MOF coated electrode with acetonitrile leads to an increasing signal intensity of the redox process (Figure S19) because the blocked ferrocene sites are regenerate. Furthermore PXRD measurements after the CV measurements show the stability of the framework (Figure S20).<sup>12</sup>

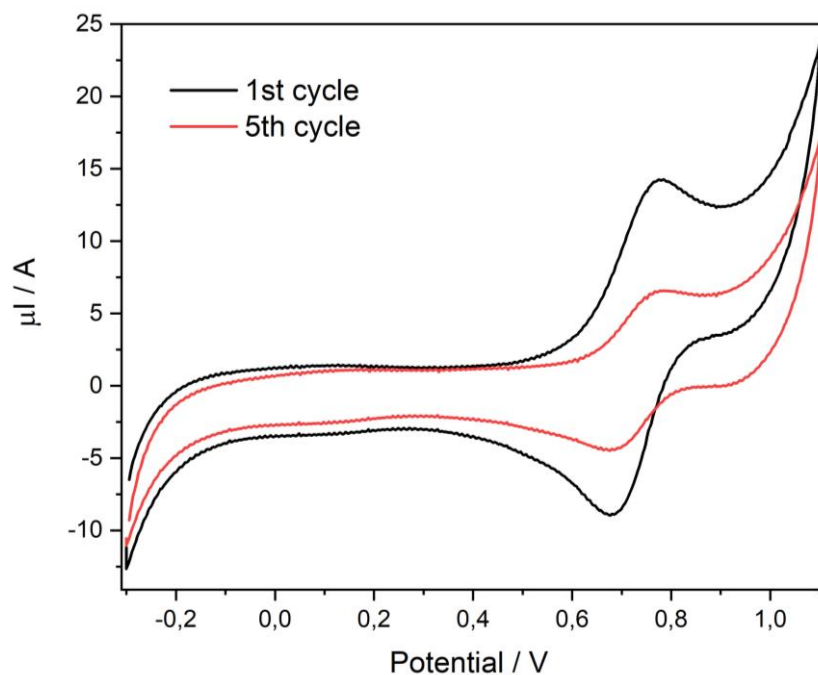


**Figure S19.** CV curve of CAU-50 (black (1st cycle) and red (5th cycle)) after washing the MOF coated gold electrode with acetonitrile. Solvent: acetonitrile, electrolyte: 0.01 mol/l  $\text{NaPF}_6$ , working electrode: gold electrode, reference electrode: Ag rod and counter electrode: Pt rod.

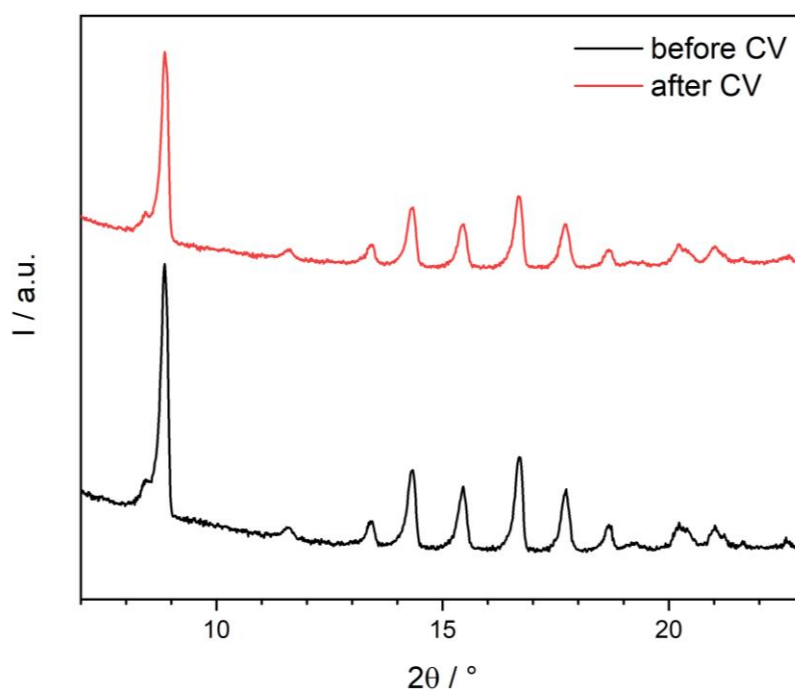


**Figure S20.** PXRD patterns of the CAU-50 deposited on gold electrode before (black) and after the CV experiment (red).

## 16 References

- 1 M. Roslova, S. Smeets, B. Wang, T. Thersleff, H. Xu and X. Zou, *Towards cross-platform automated rotation electron diffraction*, 2019.
- 2 W. Kabsch, *Acta Crystallogr., Sect. D: Biol. Crystallogr.*, 2010, **66**, 125–132.
- 3 G. M. Sheldrick, *Acta Crystallogr., Sect. A: Found. Crystallogr.*, 2008, **64**, 112–122.
- 4 W. Wan, J. Sun, J. Su, S. Hovmöller and X. Zou, *J. Appl. Crystallogr.*, 2013, **46**, 1863–1873.
- 5 *Materials Studio Version 5.0*, Accelrys Inc, San Diego, 2009.
- 6 *Topas Academics 4.2*, Coelho Software, Brisbane, 2007.
- 7 O. Knop and J. M. Hartley, *Can. J. Chem.*, 1968, **46**, 1446–1450.
- 8 a) R. T. Bailey and A. H. Curran, *J. Mol. Struct.*, 1970, **6**, 391–398; b) E. Diana, R. Rossetti, P. L. Stanghellini and S. F. A. Kettle, *Inorg. Chem.*, 1997, **36**, 382–391; c) S. Olejnik, *Clays Clay Miner.*, 1971, **19**, 83–94; d) G. Socrates, *Infrared and Raman characteristic group frequencies. Tables and charts*, Wiley, Chichester, 3rd edn., 2010;
- 9 a) H. B. Gray, Y. S. Sohn and N. Hendrickson, *J. Am. Chem. Soc.*, 1971, **93**, 3603–3612; b) M.-M. Rohmer, A. Veillard and M. H. Wood, *Chem. Phys. Lett.*, 1974, **29**, 466–468;
- 10 R. Prins, *Mol. Phys.*, 1970, **19**, 603–620.
- 11 a) M. Reiners, D. Baabe, P. Schweyen, M. Freytag, P. G. Jones and M. D. Walter, *Eur. J. Inorg. Chem.*, 2017, **2017**, 388–400; b) P. Schwerdtfeger, T. Söhnel, M. Pernpointner, J. K. Laerdahl and F. E. Wagner, *J. Chem. Phys.*, 2001, **115**, 5913–5924;
- 12 J. Benecke, E. S. Grape, A. Fuß, S. Wöhlbrandt, T. A. Engesser, A. K. Inge, N. Stock and H. Reinsch, *Inorg. Chem.*, 2020, **59**, 14, 9969 - 9978.